Simulation and optimization of a double THGEM detector

WANG Xiaohu[1, 2,*] WEI Tao[2] LONG Jidong[2] LI Quanwei[1] ZHANG Linwen[2]

[1]*Fundamental Science on Nuclear Waste and Environmental Security Laboratory, Southwest University of Science and Technology, Mianyang 621010, China*

[2]*Institute of Fluid Physics, China Academy of Engineering Physics, Mianyang 621900, China*

Abstract A double thick GEM (THGEM) detector with thin THGEM foils and small holes was constructed. In order to optimize the operation parameters of the detector, a simulation study of the detector was carried out using ANSYS and Garfield program. Some important characteristics, including primary electron transparency, avalanche development and the secondary electron loss were calculated. Parameters, such as electric field and gas choice were optimized.

Key words Micropattern gaseous detectors, Thick GEM, THGEM, Garfield, Simulation, Optimization

1 Introduction

Gas Electron Multipliers (GEMs)[1] are widely used in particle position detections with good spatial resolutions, fast time responses, high counting capabilities, etc. As an expansion of standard GEM, thick GEMs (THGEMs)[2] based on PCB techniques have more advantages than the standard GEMs'. And the THGEMs are more robust, cheaper and easier to be made. Typical THGEMs are made of PCB plates with thickness of 0.3−1 mm, holes of 0.2−1 mm in diameter, hole pitch of 0.7–1.2 mm and rim of 0−0.1 mm[3-4]. The characteristics of the THGEM detector strongly depend on the geometry of the THGEM foils and the operating parameters of the detector.

A double THGEM detector with thin THGEM foils and small holes was constructed. A systematic simulation of the detector was carried out to know more about the characteristics of the detector and optimize the detector's operation parameters.

2 THGEM detector

The structure of the THGEM detector is shown in Fig.1. The active area of the detector is 5 cm×5 cm. There are two THGEM foils, placed between a cathode plane and a readout plane. The distance between the two THGEM foils is 3 mm. The cathode plane is placed 3.8 mm up the upper THGEM foil, while the readout plane is placed 2 mm below the lower THGEM foil. The THGEM foils are made of PCB plate of 0.2 mm thick, with 18 μm copper coat on the both side of the thin plate. The holes are cylindrical in shape with diameter of 0.2 mm and rim of 20 μm. The holes were arrayed hexagonally and the pitch between each two holes is 0.5 mm.

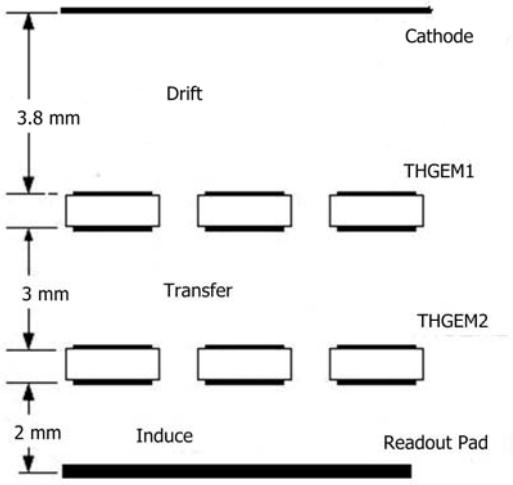

Fig.1 Structure of the THGEM detector.

Supported by Fundamental Science on Nuclear Waste and Environmental Security Laboratory, Southwest University of Science and Technology. (Grant No.11zxnk03)

* Corresponding author. *E-mail address:* wang07013@163.com

Received date: 2012-06-28

3 Simulation methods

3.1 Detector modeling

The structure of the detector, including foil geometry, dielectric constants and high voltages of the electrodes were defined by the ANSYS program. Using the finite element method (FEM), the ANSYS program divides the detector volume into a large number of small elements, and the 3D electric field of the detector can be preciously calculated if the elements are small enough. When the calculation finished, the program generates a number of output files including a 3D field map of the detector, and this field map can be read by the Garfield[5] program for further simulation. In the calculation, a small base cell shown in Fig.2 was chosen, so as to avoid the oversize of the output files. The complete THGEM foil was obtained by a symmetry operation of the base cell.

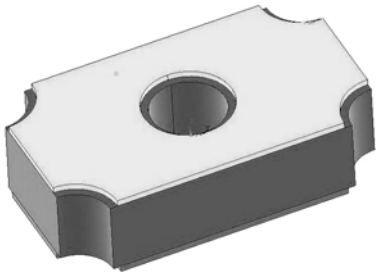

Fig.2 Base cell defined in ANSYS program for 3D electric field calculation.

3.2 Electron drift and avalanches

Garfield program was employed to simulate the electron drift and avalanche properties of the detector. Garfield could not directly define the 3D geometry of the detector, so 3D electric field maps created by ANSYS were fed to the Garfield.

In Garfield, the electron drift velocity, diffusion, Townsend and attachment coefficient of the gas mixtures was calculated by the MAGBOLTZ interface. The two subroutines DRIFT_ELECTRON_3 (Runge-Kutta method) and DRIFT_MC_ELECTRON (Monte-Carlo method) can be called to compute the end positions of all drift electrons and the results can be used to calculate the electron transparency of the detector. The electron multiplication properties in the THGEM holes were calculated by the AVALANCHE and MICROSCOPIC_AVALANCHE subroutines. The gas gain, second electron loss and avalanche shape can also be investigated by these two subroutines.

4 Simulation results

4.1 Electron collection efficiency

Only when an electron entering the THGEM hole can it trigger an avalanche and be contributing to the output signals of the detector. For the THGEM detector shown in Fig.1, the electron collection efficiency of THGEM1 and THGEM2 will both affect the detector's output signals. Normal used gas mixture Ar/CO_2(70/30) under room temperature and atmospheric pressure was used in this section.

4.1.1 Primary electron collection efficiency of THGEM1

In the simulation, a number of electrons were drifted from a plane 0.8 mm below the cathode plane, and the start positions were uniformly selected in the area corresponding to the base cell shown in Fig.2. According to the end positions of the drift electrons, we can judge if the electron was hit on the metal surface, or hit on the PCB dielectric substrate, or passed through the hole, and therefore the electron collection efficiency can be obtained.

We define the probability that an electron can drift into the whole region of the THGEM1 as E_{c1}. By our calculation, E_{c1} strongly depends on the electric field of the drift region (here defined as *E*-drift), but are almost not influenced by the electric field of the transfer region (here defined as *E*-transfer). As shown in Fig.3, the electron collection efficiency of THGEM1 keeps close to 100% if *E*-drift is ranged from 0 to 400 $V \cdot cm^{-1}$. However, as E-drift increases, the electron transparency decreases because more and more electrons will hit the upper surface of THGEM1 rather than drift into the holes.

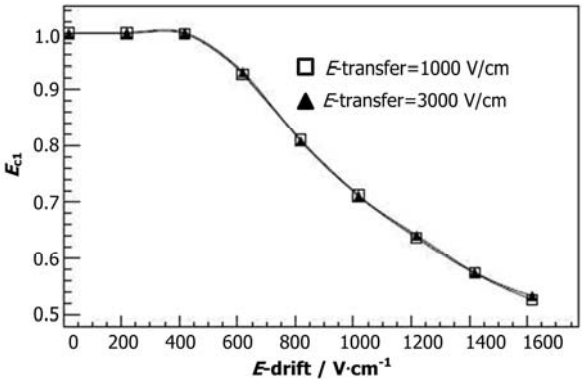

Fig.3 Primary electron collection efficiency of THGEM1 as a function of *E*-drift.

4.1.2 Electron collection efficiency of THGEM2

The electron collection efficiency of THGEM2 is defined as E_{c2}, which means the ratio of the number of the electrons that passed through the holes of THGEM1 to the number of electrons drift into holes of THGEM2. After passing through the THGEM1 hole, an electron can either hit the lower metal surface of THGEM1, or lost in transfer region, or hit the upper metal surface of THGEM2, or drift into holes of THGEM2. Which process it will undergo is mainly determined by the electric field of the transfer region, but is weakly affected by the E-drift and E-induce (electric field of the induce region). The influence of E-transfer on the electron collection efficiency of THGEM2 is shown in Fig.4. By our calculation, we found that, a large number of electrons will end on the lower metal surface of THGEM1 if E-transfer is very small, but as E-transfer increases the number of electrons that hit the upper surface of THGEM2 increases as well and the maximum of the collection efficiency (about 96%) approximately occurs at *E*-transfer=600 V·cm^{-1}. However, this is not the case for the collection of secondary electrons generated in THGEM1 holes, because the probability whether a secondary electron can pass through the THGEM1 hole is although affected by E-transfer, as will discuss below.

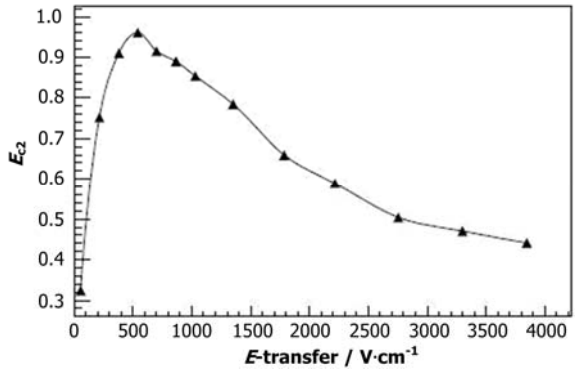

Fig.4 Influence of E-transfer on electron collection efficiency of THGEM2.

4.2 Avalanche performances

4.2.1 Gas multiplication factor for single THGEM foil

The multiplication factor of the THGEM can be calculated with the AVANLANCHE subroutine in Garfield. For the double THGEM detector, the calculated multiplication factor is only 3×10^3 in Ar/iC_4H_{10} (97/3) for V-gem of 500 V. The value is far less than the experimental results, which is about 4.6×10^4. The big difference between simulation and experiment in gas multiplication factor originates from the Monte Carlo step dependence in gain calculation in Garfield, as is mentioned in Refs.6-8. Therefore, the calculated gas multiplication factor is meaningless for us, and what we will focus on is the secondary electron loss and the avalanche spatial distribution and gas mixture dependence of the multiplication factor, as will discuss below.

4.2.2 Secondary electron collection efficiency

Here we define the secondary electron extraction efficiency E_{s1} as the probability that a secondary electron can escape from the THGEM1 holes and go to the next electrode plane. Fig.5 is a typical end position distribution of secondary electrons. In the simulation, the THGEM1 foil was placed in *X*-*Y* plane with coordinate of *Z*=0. Considering the thickness of THGEM foil and the metal surface, secondary electron with *z*-coordinate of its end position less than −0.118 mm was considered escaped from THGEM1. As shown in Fig.5, about 60% of the secondary electrons can escape from the THGEM1 holes when v-gem1 is 500 V and E-transfer is 3000 V·cm^{-1}.

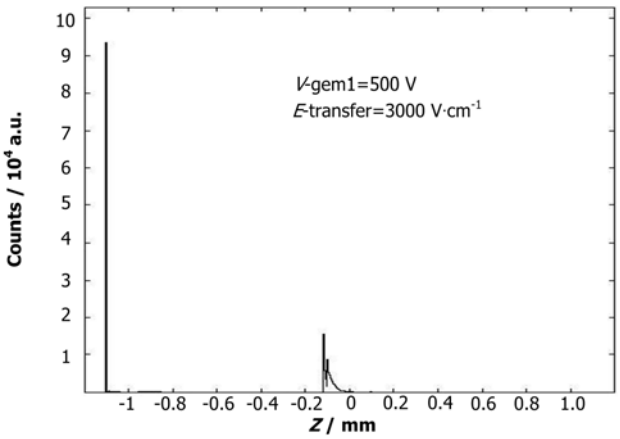

Fig.5 End position distribution of the second electrons, with *V*-gem1 of 500 V and *E*-transfer of 3000 V·cm^{-1}.

The dependence of the secondary electron extraction efficiency E_{s1} on *V*-gem and *E*-transfer is shown in Fig.6. It can be seen that E_{s1} increases rapidly with the increase of *E*-transfer, but it is almost

not influenced by V-gem1. This result shows that, the higher the electric field below the THGEM is, the easier the secondary electrons can escape from the THGEM holes. If the electric field below the THGEM foil was set to 5000 V·cm^{-1}, more than 75% of the secondary electrons can be extracted from THGEM holes. For standard GEM with kapton foil thickness of 50 μm, the value is typically ~30−60%[6,7], so generally the secondary electron extraction efficiency of THGEMs is higher than that of standard gems.

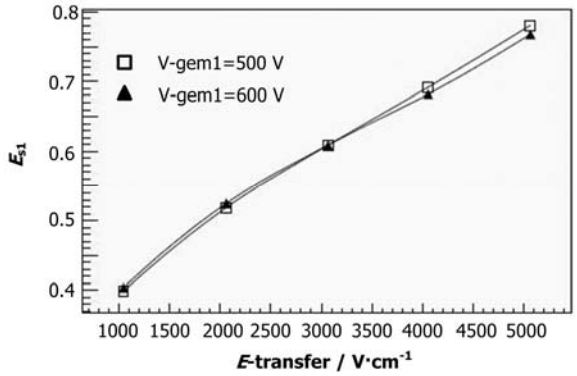

Fig.6 Dependence of the secondary electron extraction efficiency of THGEM1 (E_{s1}) on *E*-transfer, for *V*-gem1 of 500 V and 600 V, respectively.

The total second electrons that can reach the hole region of THGEM2 is determined both by secondary electron extraction efficiency of THGEM1 (E_{s1}) and the electron collection efficiency of THGEM2 (E_{c2}). So the product $E_{s1}\times E_{c2}$ can be used to describe the effective secondary electron collection efficiency of THGEM2. As mentioned above, E_{s1} and E_{c2} are almost only affected by *E*-transfer, so the influence of *E*-transfer on $E_{s1}\times E_{c2}$ was calculated. In Fig.7, $E_{s1}\times E_{c2}$ increases with the increase of *E*-transfer when *E*-transfer is small, and it reaches its maximum when *E*-transfer increases to about 1500 V·cm^{-1}. However, the variation of $E_{s1}\times E_{c2}$ is relatively small when *E*-transfer is larger than 500 V·cm^{-1}. Therefore, *E*-transfer of larger than 500 V·cm^{-1} is necessary for the effective collection of the secondary electrons of THGEM1.

As for the secondary electron extraction efficiency of THGEM2 (here defined as E_{s2}), similar to E_{s1}, it is mainly determined by *E*-induce. From Fig.6, we can deduce that, for the higher secondary electrons extraction efficiency of THGEM2, *E*-induce should be the larger the better, but it is obviously limited by the electric discharge of the detector.

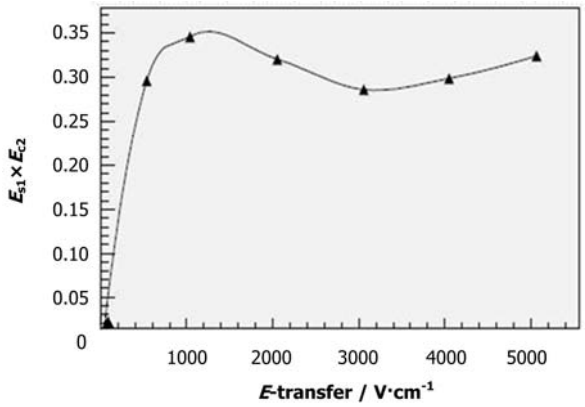

Fig.7 Influence of *E*-transfer on the effective secondary electron collection efficiency of THGEM2.

4.2.3 Complete avalanche process of the detector

The avalanche shape of the detector is an important factor for the determination of the dimension of the readout strips (or pads). The complete avalanche development of the detector was calculated. In the calculation, a number of electrons, simulated as the primary electrons generated by an X-ray particle, were made drift from a point 2 mm up from the upper surface of THGEM1. The avalanche processes for Ar/isobutance (97/3) and Ar/CO_2 (90/10) were shown in Fig.8. The calculation results show that gas mixture Ar/isobutance (97/3) not only has a much higher multiplication factor than Ar/CO_2(90/10), but also has a wider avalanche spatial distribution. From Fig.8, it can be found that, in Ar/isobutance(97/3), which has a larger transverse diffusion coefficient than Ar/CO_2(90/10), the width of secondary electron distribution on the readout plane is about 3 mm, comparing to the width of only about 1.5 mm for Ar/CO_2(90/10).

Since a wider secondary electron distribution on the readout plane implies much less readout channels, the gas mixtures of larger transverse diffusion coefficient are more acceptable for this type of detectors.

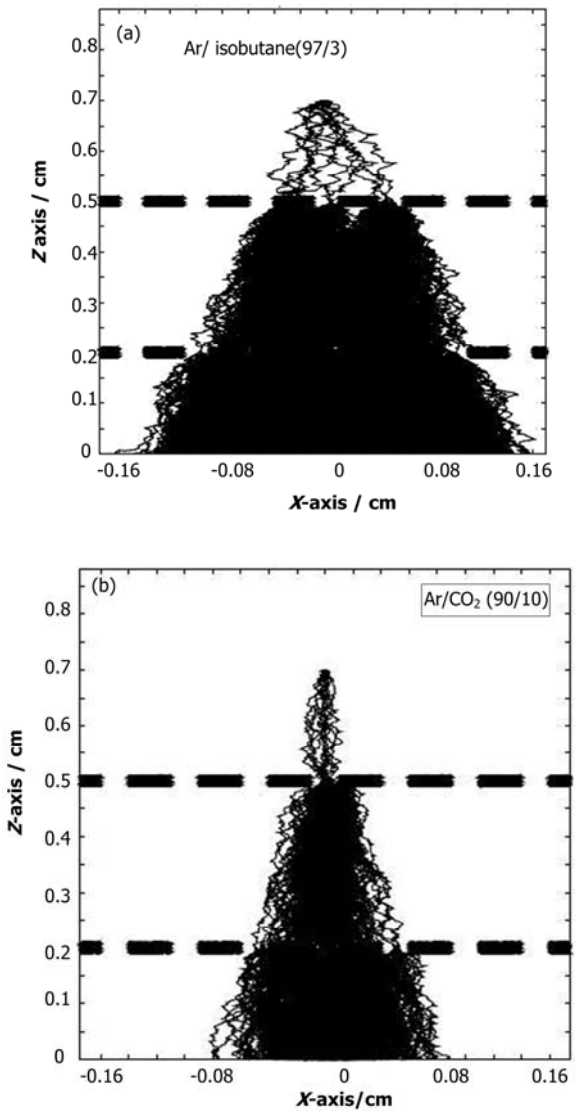

Fig.8 Avalanche development of the detector in Ar/isobutance(97/3) (a) and in Ar/CO_2(90/10) (b).

5 Conclusion

Behavior of a double THGEM detector was simulated. From the simulation result, following rules should be taken for the optimization operation of the detector.

The electric field of the drift region (*E*-drift) should be smaller than 400 V·cm^{-1}, so as to obtain a nearly 100% primary electron collection efficiency. The electric field in the transfer region (*E*-transfer) of larger than 500 V·cm^{-1} is needed, for the effective collection efficiency of the secondary electrons generated in THGEM1 holes. As for *E*-induce (electric field in the induce region), in order to get a higher secondary electron extraction efficiency of THGEM2, it should be the larger the better. Finally, for the minimization of readout channels, gas mixture with large transverse diffusion coefficient is more acceptable for the detector.

Acknowledgments

We thank Prof. Xie Yigang from Graduate University of Chinese Academy of Sciences for providing the THGEM foils.

Referances

1 Sauli F. Nucl Instrum Meth A, 1997, **368:** 531−534.

2 Chechika R, Breskin A, Shalem C, *et al.* Nucl Instrum Meth Phy Res A, 2004, **535:** 303−308.

3 Alexeev M, Birsa R, Bradamante F, *et al.* Nucl Instrum Meth Phy Res A, 2010, **617:** 396−397.

4 Breskin A, Cortesi M, Alon R, *et al.* Nucl Instrum Meth Phy Res A, 2010, **623:** 132−134.

5 Garfield V R. A Drift-Chamber Simulation Program. http://garfield.web.cern.ch/.

6 Bouianov O, Bouianov M, Orava R, *et al.* Nucl Instrum Meth Phy Res A, 2000, **450:** 277−287.

7 Bouianov O, Bouianov M, Orava R, *et al.* Nucl Instrum Meth Phy Res A, 2001, **458:** 698−709.

8 Tikhonov V, Veenhof R. Nucl Instrum Meth Phy Res A, 2002, **478:** 452−454.